Journal of Marine Research, 59, 921–948, 2001

Central equatorial Pacific zonal currents. II: The seasonal cycle and the boreal spring surface eastward surge

by D. E. Harrison[1,2], R. D. Romea[1] and G. A. Vecchi[1,2]

ABSTRACT

The seasonally averaged zonal momentum equation tendencies at 140W are studied in a high-resolution primitive equation ocean general circulation model simulation of the tropical Pacific. The model experiment, forced by climatological monthly average wind-stress, reproduces well the observed boreal springtime eastward surge of the normally westward surface flow, as well as many features of the acceleration and deceleration between the surface and 200 m between January and October. We present each of the zonal momentum equation tendency terms for the depth range 0–160 m, but our discussion focuses on the behavior of the boreal springtime near-surface flow, perhaps the most distinctive feature of the seasonal cycle. The eastward surface surge in boreal spring depends crucially on the springtime weakening of the otherwise westward tendency from tropical instability waves (TIWs). The TIW effects, together with the eastward tendency from the seasonal weakening of the easterly wind-stress, drive the eastward surface current surge. Although the 'negative viscosity' effect of the TIWs is small in the annual mean, as we have previously shown, its seasonal variation is necessary to the surface flow reversal and eastward surge in this model. A series of experiments, each with weaker TIWs than its predecessor, shows a progressive weakening and eventual absence of springtime eastward surface flow, supporting the above analysis. The seasonal zonal velocity accelerations and decelerations are small compared with the terms in the zonal momentum equation; these terms must be known to an accuracy of at least 10 cm s^{-1} $month^{-1}$ (2–5% of the largest terms) if a meaningful budget is to be obtained. This is a strong constraint that must be planned for in future observational studies. We find that nonlinear terms are $O(1)$ in the vertically-integrated balance as well as the local balance, in contrast with some recent observational estimates. Extrapolated velocity errors, neglected terms, data processing assumptions, and crude finite-differencing in the observational studies may account for the differences, as appeared to be the case in the annual mean balances. The model dynamical balances cannot be reproduced if the methods used to analyze observational data are applied to the model output fields. Very near-surface currents must be measured rather than extrapolated if the ocean shear is similar to that of the model flows.

1. Introduction

The dynamics of equatorial currents, mean and time-dependent, have interested oceanographers since the 1940s. Simple dynamical balances have led to a qualitative understand-

1. PMEL/NOAA, 7600 Sand Point Way, NE, Seattle, Washington, 98115, U.S.A. ***email: harrison@pmel.noaa.gov***

2. Joint Institute for the Study of the Atmosphere and Ocean (JISAO), University of Washington, Box 354235, Seattle, Washington, 98195, U.S.A.

ing of many aspects of equatorial flows (e.g., Sverdrup, 1947; Gill, 1982). Harrison *et al.* (2001; hereafter HRH) recently surveyed observational estimates and presented high-resolution ocean GCM results for the annual mean dynamical balances of zonal currents in the central equatorial Pacific Ocean. We here extend that study to the seasonal cycle of zonal currents in the same region, through examination of the zonal momentum equation tendency terms in seasonally varying ocean GCM experiments, and comparison with observational estimates.

Yu and McPhaden (1999a; hereafter YMa) have described currents and surface winds from nine years of measurements from the equatorial moorings of the Tropical Atmosphere Ocean (TAO) buoy array (McPhaden, 1989). At 140W the seasonal cycle of surface winds involves easterly (from the east) trade-winds except at the height of major El Niño events, with weakest easterlies in the month of March in the climatological seasonal cycle. The most striking feature of the seasonal cycle of the currents is the boreal springtime period of eastward flow (counter to the prevailing easterly winds); nine to ten months of the year the surface flow is westward. During the period of surface eastward acceleration there is a period of eastward subsurface acceleration, down to the core of the Equatorial Undercurrent (EUC). The change in upper-EUC speed is typically about 20% of the mean speed, while the seasonal cycle in the lower EUC is even smaller and has different timing from the shallower changes. The springtime eastward near-surface surge is the only $O(1)$ change in the seasonal cycle.

Two recent papers have examined seasonal aspects of the zonal momentum balances using observations. Yu and McPhaden (1999b; hereafter YMb), and Qiao and Weisberg (1997; henceforth QW). YMb found that for the seasonal cycle of the upper 250 m of the equatorial Pacific between 110W and 170W, the zonal surface wind-stress and pressure gradient roughly balanced (the equatorial Sverdrup balance; Sverdrup, 1947; Gill, 1982) in the depth-integrated zonal momentum balance. Currents shallower than 30 m were extrapolated from 30–40 m currents and shear. Because of the limited data set, they were not able to estimate the meridional and vertical zonal momentum advection terms.

QW described the zonal momentum balances of the upper equatorial Pacific Ocean using data taken from five ADCP moorings deployed in a diamond-shaped array about (140W, 0N) over 13 months, as part of the Tropical Instability Wave Experiment (TIWE). The three equatorial moorings were at 142W, 140W, and 138W, and the two off-equatorial moorings were located at (140W, 1S) and (140W, 1N). Measurements above 30 m depth were contaminated by surface effects, so the velocity field was estimated there by linear extrapolation using the shear between 30 and 40 m. The array was designed to provide a three-dimensional view of the circulation; the vertical velocity $w(z)$ was estimated by vertically integrating the finite differenced horizontal divergence between the surface and depth z. The horizontal derivatives were computed with central differences, so that $\Delta\theta = 4°$ (Longitude) and $\Delta\varphi = 2°$ (Latitude). QW cannot evaluate all the zonal momentum equation terms either, but the analysis is more comprehensive (for its time interval) than that of YMb. However, as they state in their discussion section: "The analyses presented

for the time-dependent zonal momentum balance were more qualitative." They find that nonlinearity is strongest within the EUC core region. While the individual nonlinear terms are comparable in magnitude with the local acceleration, they tend to cancel upon vertical integration. They find that, in a vertically integrated sense, the equatorial Sverdrup balance roughly holds over the depth interval of the surface to the main thermocline; thus, the mass transport depends roughly linearly on wind-stress changes.

We here extend the HRH analysis of the zonal momentum equation term balances of a primitive equation ocean general circulation model experiment that reproduces many aspects of the observed zonal currents.[3] This experiment produces currents with central Pacific TIW amplitudes, EUC speeds and seasonal eastward surface currents as realistic as any known to us. The seasonal climatological currents and their dynamics, and how these compare with the reported observational currents and balances will be described. While there are some discrepancies between the model currents and the observed currents, the basic features and amplitudes of the observations are well reproduced in the model experiment. The model system gives us the ability to evaluate fully the terms in the model zonal momentum equation (including those which could not be evaluated in the observational studies above).

As mentioned above, we focus our discussion on the boreal spring surface current reversal; it is a distinctive aspect of the seasonal cycle, involving the largest relative amplitude changes in current speed. The full seasonal cycle between the surface and the subcore part of the EUC exhibits a wide range of dynamical balances; a complete description of them would make this paper unwieldy to the reader. As we found in the annual mean, the seasonal climatological model dynamical balances differ in some basic ways from the estimated observed balances. Because of the limitations of the observational data sets and the analyses of them, additional observations will be needed before the skill of the model balances can be evaluated. The model balances are, however, plausible and the model-observational balance differences can be explained at least qualitatively through subsampling the model currents as if they were observed with the instruments and mooring spacing used in the TIWE array, and then analyzing them with crude finite differencing, as was done by QW. This process is described more fully in Section 3 below.

There has been previous modeling work on the seasonal cycle of equatorial Pacific zonal currents. Philander *et al.* (1987) presented snapshots of the near-surface zonal flow at several longitudes from a seasonal cycle experiment using the same primitive equation general circulation model used here (with a different surface wind-stress field), however they did not examine the dynamical balances responsible for the flows. It is difficult to compare the Philander *et al.* (1987) snapshots with the seasonally-averaged flow results that are the focus here. Philander and Chao (1991; henceforth PC91) presented some schematic dynamical balances for two snapshots in the seasonal cycle at 140W, 0N from a

3. For a complete description of the model and the model experiment, including the annual mean balances and their comparison with observations, see Harrison *et al.* (2001, this issue).

Philander *et al.* (1987)-type experiment, but presented no detailed examination of the zonal momentum terms through the seasonal cycle. Our model better resembles the seasonal observations than do the recent results of Yu *et al.* (1997) (hereafter Yu97). Using a different ocean model with less vertical resolution, their flow also has TIW energy and exhibits eastward near-surface flow in the boreal spring, but their EUC has substantially greater maximum speed and rather different upper ocean vertical shear than observed. They did not provide zonal momentum equation diagnostics, but only state: "At this time (boreal spring) weakened local easterlies cause anomalous eastward flow that reverses the westward surface current and intensifies the EUC. Conversely, in late summer and fall strengthened local easterlies enhance the SEC and weaken the EUC (p. 323)." They do not explain how the wind changes bring about the current changes.

Our analysis of our model results indicates that the momentum tendency of the TIWs, through changes in their meridional advection of zonal momentum, is a crucial process that enhances the wind-driven, near-surface eastward acceleration and leads to the springtime surface current reversal. The PC91 and Yu97 model results exhibit at least some TIW amplitude, but the TIW effects on the seasonal variation of currents are not discussed. It would be very interesting to know more about the changes in advection, mixing and pressure gradients that produce the Yu97 seasonal upper ocean flow reversal. We believe the analysis presented here will likely also hold for the PC91 experiment, because of the similarity between the two models and the forcing used.

The next section summarizes our seasonal cycle results; low-pass filtering defines the seasonal signal. Section 3 presents a discussion of the seasonal zonal momentum equation balances with emphasis on the spring surface current reversal period. Nonlinear terms in the zonal momentum balance resulting from TIWs are shown to be critical drivers; a discussion of the significance of TIWs in driving the spring-time reversal of the near-surface South Equatorial Current, is presented in Section 4. Section 5 presents our discussion and conclusions.

2. Seasonal cycle of the zonal flow at 140W

Figure 1 shows several views of the time variation of zonal velocity (u; positive eastward) between the surface and 240 m at (140W, 0N) over one year of the model simulation; Figure 1a shows snapshots of the model zonal flow every 3 days; Figure 1b shows the same data after time-smoothing with a seasonal (60 day Cosine) filter. This filter is successful at greatly reducing the velocity components of the energetic TIW flows that are clear in Figure 1a. With this approach, filtered terms (denoted with subscript "s") contain the seasonal signal and the annual mean. The residual, which represents fluctuations with periods shorter than about 90 days, including contributions from TIWs, is represented by u', i.e.,

$$u = u_s + u'. \tag{1}$$

As in the observations, the eastward zonal flows at the surface and at the core of the EUC

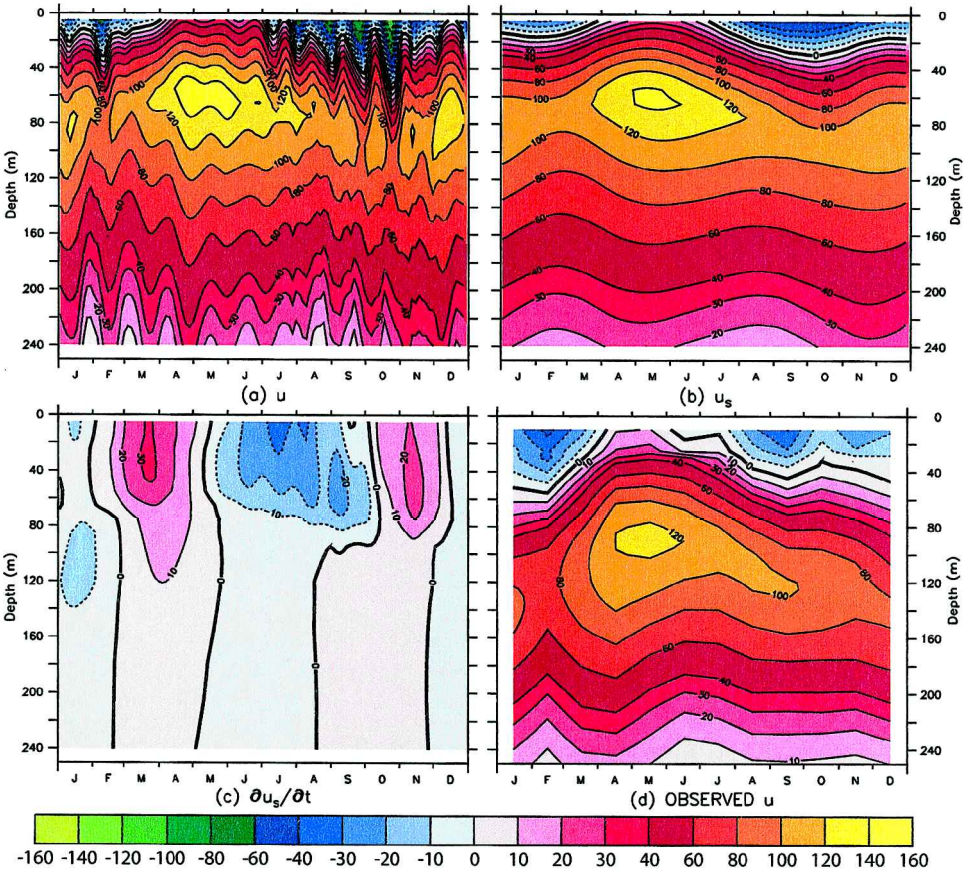

Figure 1. Time evolution of equatorial upper ocean zonal velocity (u; cm/s; positive eastward) at (140W, 0N) between the surface and 250 m, from one year of the climatological seasonal cycle simulation: (a) u 'snapshots' every 3 days, (b) seasonally-filtered u_s (60 day Cosine filter; eliminates the zonal component of the energetic TIW flows that are clear in Fig. 1a.), (c) time derivative ($\partial u_s/\partial t$; cm/s/month) of the model seasonal zonal velocity, (d) observed climatological monthly average zonal velocity (cm/s) from an upward-looking acoustic Doppler profiling current meter (ADCP) mooring at (140W, 0N) over the period 1990–1998 (Yu and McPhaden, 1999a). 'Cool' colors denote westward flow; 'warm' colors denote eastward flow.

are strongest in May; they are weakest in October. In November–December there is a weak secondary eastward maximum in the model EUC flow. Figure 1c shows the time evolution ($\partial u_s/\partial t$), in cm/s per month, of the filtered seasonal zonal flow (t is time). The strongest accelerations occur in phase in the vertical between the surface and somewhat above the core of the EUC. The eastward acceleration that leads to the reversal of the surface flow in late boreal spring extends to about the depth of the core of the model EUC. The near-surface eastward acceleration begins in February, reaches maximum intensity in

March and is gone by early May. Other acceleration also occurs nearly in phase between about 100 m and 250 m but more weakly and later than for the shallower region.

Figure 1d presents the climatological monthly mean zonal flow from an upward-looking acoustic Doppler profiling current meter (ADCP) mooring at (140W, 0N) over the period 1990–1998 (Yu and McPhaden, 1999a). Currents shallower than 30 m have been extrapolated based on shears at the upper bin of the ADCP data. We have verified that the inclusion of older mechanical current meter observations from the 1980s (McPhaden and Hayes, 1990) does not introduce qualitatively new features. The major features of the seasonal cycle from January to October are present in the model results. The model EUC is 5–10% stronger and the interval of model eastward surface flow lasts about 1 month more than in the observed climatology. The second period of acceleration (November–December), seen in the model, is much less evident in the observations and will not be given much attention here.

To examine the representativeness of the observed climatology, consider Figure 2, which shows the seasonally smoothed ADCP data from each of the years 1991 to 1994. The spring eastward near-surface flow existed in most years but its duration varied by as much as two months. The spring maximum in the EUC is also a relatively robust feature, but the peak speed differs year-to-year by up to 50 cm/s. There are periods of EUC acceleration in autumn in many years, but they occur less regularly. This may explain why the model's second acceleration period is 'washed-out' in the YMa observed climatology. This region has strong interannual variability, introducing significant uncertainty in a climatology derived from a relatively short record. The differences between the model results and observations are smaller than 20% in the EUC, which we believe is better than any previously published comparison. Because there are no direct observations of the surface flow, it is not possible to say how realistic the model flow at the surface is.

The meridional structure of the model surface zonal flow reversal is shown in Figure 3. Figures 3a and b present the 3-day sampled (u) and seasonally filtered (u_s) zonal surface flow from the model (surface model grid point; 5-m depth), at 140W; note that the near-equatorial instability waves have their maximum zonal flow between 1N and 2N and that they are far more energetic north of the equator than south of it. Figures 10 and 11 of HRH provide details of the time-averaged properties of the TIW momentum fluxes. The period of spring eastward surface current is contemporaneous with the seasonal weakening of TIW activity. The filtered time series (Fig. 3b) shows that strong changes occur in the seasonal zonal flow all across the waveguide, 3N to 3S, although the largest changes occur near the equator. The spring current reversal is confined to within 1.5S–1N, while the weakening of TIW activity extends to 4N. Figure 3c shows the time derivative ($\partial u_s/\partial t$) of the seasonal surface zonal flow; for the spring (Feb–May) eastward acceleration period, the main accelerations and decelerations occur first on the equator and later at higher latitudes.

For reference, the seasonally filtered waveguide zonal (τ_s^x) and meridional (τ_s^y) wind-stress forcing fields are presented in Figures 4a and 4b, respectively. The zonal wind-stress is always directed to the west; although the easterly stress weakens prior to the spring

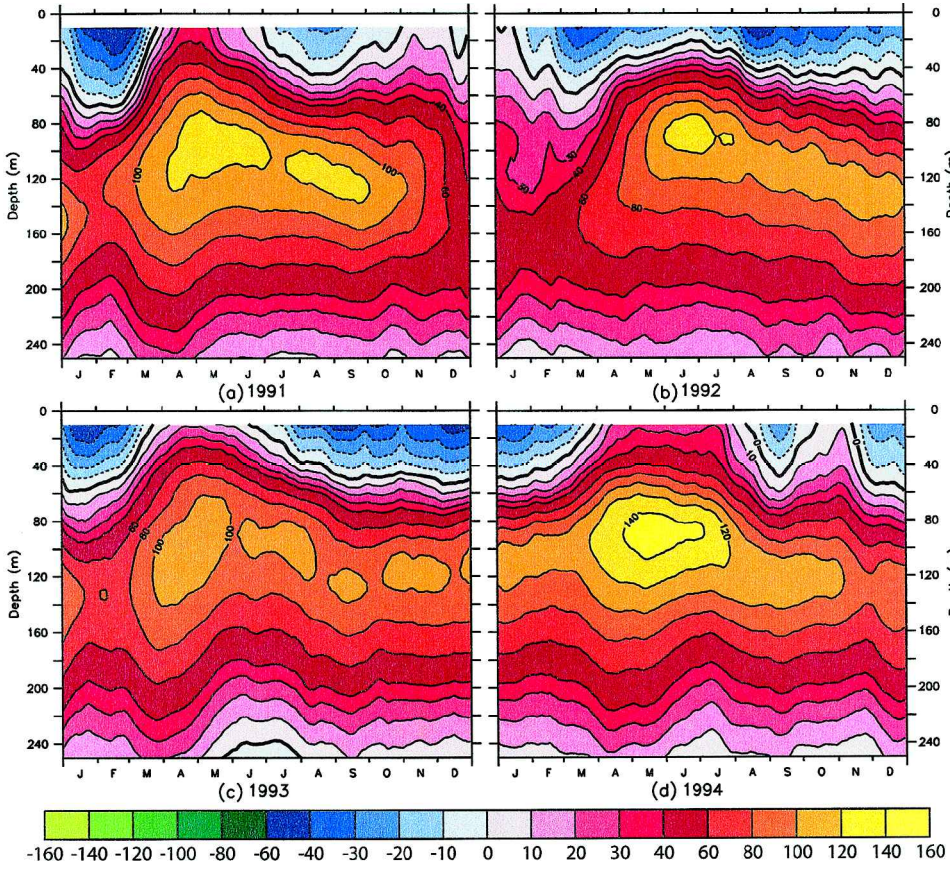

Figure 2. Seasonally smoothed equatorial upper ocean zonal velocity (u; cm/s; positive eastward) from an upward-looking acoustic Doppler profiling current meter (ADCP) mooring at (140W, 0N) between the surface and 250 m (Yu and McPhaden, 1999a). Data are shown for the years (a) 1991, (b) 1992, (c) 1993 and (d) 1994.

surface current reversal, we shall show that this wind-stress forcing alone cannot drive an eastward surface equatorial current in the model. The model zonal stress also weakens somewhat during Aug–Oct. Note that the zonal stress between February and July has little meridional structure, but that between July and October τ_s^x weakens significantly north of the equator and between October and December it strengthens significantly south of the equator. The meridional stress exhibits little meridional structure between February and June and then a substantial gradient forms later in the summer, as τ_s^y increases sharply north of the equator but not south of it. The climatological wind data produce a very noisy wind-stress curl field, and it is not shown. If the wind-stress data are smoothed by zonal averaging over 10° of longitude and 2° of latitude, as was done by Wyrtki and Meyers

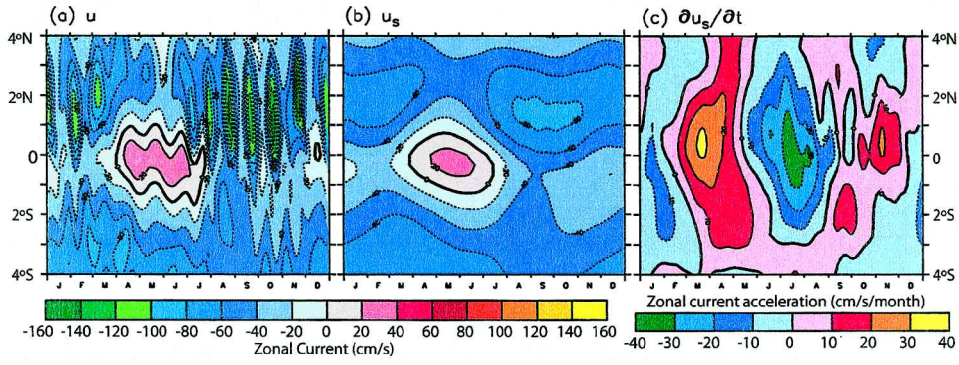

Figure 3. Meridional structure (4S to 4N) of the model surface zonal flow (u; cm/s; positive eastward), at 140W: (a) 3-day 'snapshots,' (b) seasonal cycle u_s, (c) time derivative ($\partial u_s/\partial t$; cm/s/month) of the seasonal zonal velocity. Note that (a) and (b) have the same contour intervals, while (c) has different contour intervals.

(1976), the curl field becomes contourable and is shown as Figure 4c. There are large variations in the curl poleward of 2N.

3. The seasonal zonal momentum equation balances

We now explore the processes that affect the spring surface zonal current reversal in the seasonal cycle by examining the terms in the zonal momentum equation:

$$\frac{\partial u}{\partial t} = -\left(u\frac{\partial u}{\partial x} + v\frac{\partial u}{\partial y} + w\frac{\partial u}{\partial z}\right) - \frac{1}{\rho}\frac{\partial p}{\partial x} + fv + A_{mH}\left(\frac{\partial^2 u}{\partial x^2} + \frac{\partial^2 v}{\partial y^2}\right) + \frac{\partial}{\partial z}\left(A_{mV}\frac{\partial u}{\partial z}\right) + \frac{\partial}{\partial z}\left(\frac{\tau^x}{\rho}\right)\delta_{i1}, \tag{2}$$

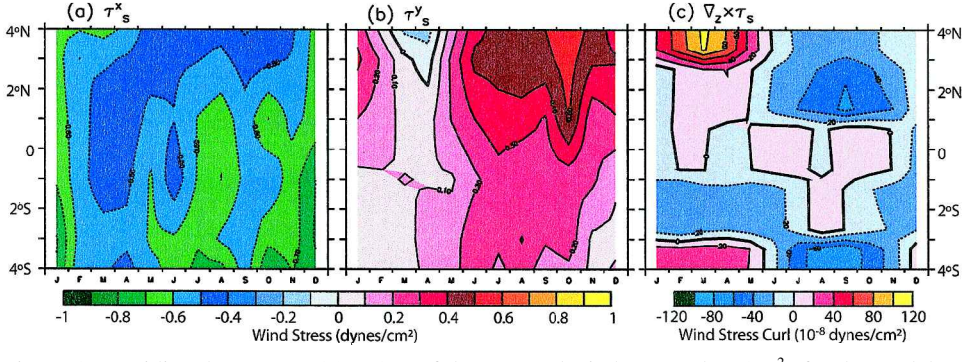

Figure 4. Meridional structure (4S to 4N) of the seasonal wind-stress (dyne/cm^2) for the model, at 140W: (a) zonal wind-stress (τ^x_s; positive eastward), (b) meridional wind-stress (τ^y_s; positive northward), (c) wind-stress curl ($\nabla_z \times \tau_s$; dyne/cm $\times$ 10^8) averaged 2° meridionally and 10° zonally. 'Cool' colors denote westward stress (easterly); 'warm' colors denote eastward stress (westerly).

where t is time, ρ is density, p is pressure, f is the Coriolis parameter, and the horizontal and vertical eddy viscosities are represented as A_{mH} and A_{mV}, respectively. The grid is such that (u, x) is positive eastward, (v, y) is positive northward, and (w, z) is positive vertically upward. The equation is written such that each term on the right-hand side acts as a 'tendency' that drives the local acceleration $(\partial u/\partial t)$ of the zonal current. The last term on the right-hand side of (2) represents the contribution to the vertical mixing of the zonal wind-stress τ^x in the first vertical level ($i = 1$) of the model ($\delta_{i1} = 0$ if $i \neq 1$, $\delta_{i1} = 1$ if $i = 1$). Note that the term balances reported here are computed on the MOM spherical coordinate model grid, so that (2) is not strictly correct (cosine factors and metric terms are missing; see Pacanowski, 1995). However the notation will suffice for our discussion.

We form the seasonally filtered momentum equation by filtering (2), term by term:

$$\frac{\partial u_s}{\partial t} = -\left(u\frac{\partial u}{\partial x} + v\frac{\partial u}{\partial y} + w\frac{\partial u}{\partial z}\right)_s - \frac{1}{\rho}\frac{\partial p_s}{\partial x} + fv_s + D_{Hs} + D_{Zs}, \tag{3}$$

where the brackets denote that the quantity inside is computed, then seasonally filtered, and where we define the mixing tendencies:

$$D_{Hs} = A_{mH}\left(\frac{\partial^2 u_s}{\partial x^2} + \frac{\partial^2 v_s}{\partial y^2}\right), \tag{4}$$

$$D_{Zs} = \frac{\partial}{\partial z}\left(A_{mV}\frac{\partial u_s}{\partial z}\right) + \frac{\partial}{\partial z}\left(\frac{\tau_s^x}{\rho}\right)\delta_{i1}. \tag{5}$$

Because of the presence of both the seasonal cycle and the TIWs, the nonlinear advective terms (the total zonal momentum tendency due to advection of zonal momentum) include both the tendency from the seasonal advection by the seasonal flow (denoted below by NLA_s) and from the Reynolds Stress divergence, primarily due to TIWs (denoted by $\mathrm{NLA}_{\mathrm{TIW}}$):

$$-\left(u\frac{\partial u}{\partial x} + v\frac{\partial u}{\partial y} + w\frac{\partial u}{\partial z}\right)_s = \mathrm{NLA}_s + \mathrm{NLA}_{\mathrm{TIW}}, \tag{6}$$

$$\mathrm{NLA}_s = -u_s\frac{\partial u_s}{\partial x} - v_s\frac{\partial u_s}{\partial y} - w_s\frac{\partial u_s}{\partial z}, \tag{7}$$

$$\mathrm{NLA}_{\mathrm{TIW}} = -\left(u'\frac{\partial u'}{\partial x} + v'\frac{\partial u'}{\partial y} + w'\frac{\partial u'}{\partial z}\right)_s. \tag{8}$$

We find that there is a sufficient spectral gap between the instability wave energetic band and the seasonally varying flow that the seasonal filtering operation behaves very much like a classical Reynolds averaging operator, permitting (6).

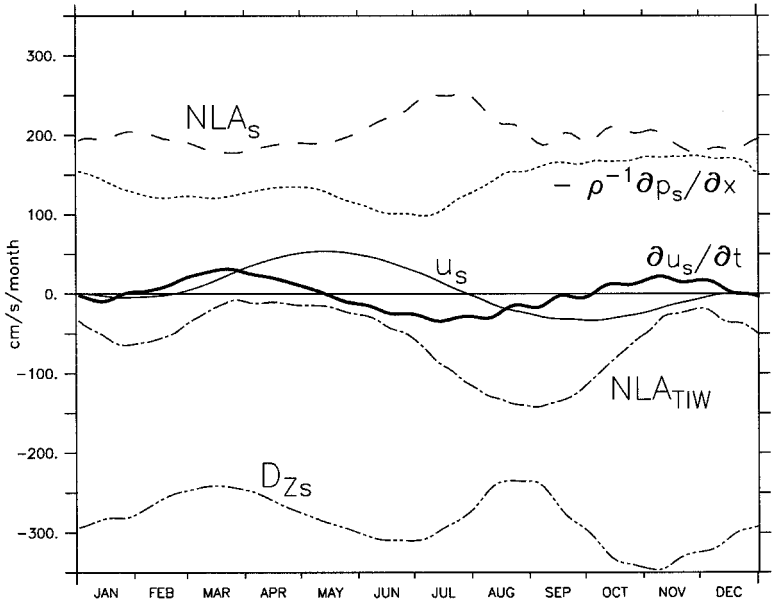

Figure 5. Tendencies in the seasonally-filtered zonal momentum equation (Eq. 3 in text) at one point: (140W, 0N), averaged over $z = 0$–30 m depth (encompassing the three near-surface grid points: 5, 15, 25 m). The term balances are shown for one model year of the seasonal cycle, in units of cm/s/month, with the convention that positive values imply a tendency toward positive $\partial u_s/\partial t$. The tendency terms representing the pressure gradient ($-\rho^{-1}\partial p_s/\partial x$), the vertical mixing ($D_{Zs}$, which includes the wind-stress forcing; Eq. 5 in text), and the seasonal (NLA$_s$; seasonal advection by the seasonal flow; Eq. 7 in text) and TIW (NLA$_{TIW}$; TIW Reynolds stress contribution; Eq. 8 in text) nonlinear accelerations are shown. The horizontal mixing tendency is not shown because its effect is negligible at this location. For reference, the zonal velocity (u_s; cm/s) and the acceleration terms ($\partial u_s/\partial t$) are also shown.

a. The near-surface momentum balances at (140W, 0N)

Because of our interest in the near-surface eastward springtime surge, we begin our examination of the term balances in the seasonal cycle with the various terms in (3) at (140W, 0N), averaged over $z = 0$–30 m depth (Fig. 5). The term balances are shown over one year of the seasonal cycle, in units of cm/s/month. The tendency terms representing the pressure gradient, the vertical mixing (which includes the wind-stress forcing), and the seasonal and TIW nonlinear acceleration terms are shown. The horizontal mixing tendency and the Coriolis tendency are not shown because their effects are negligible in this region. For reference, the zonal velocity (u_s) and acceleration ($\partial u_s/\partial t$) terms are also shown. Note that the seasonal cycle accelerations (always less than 40 cm/s/month) for this surface-and-near-surface region are typically 20% or less the size of the largest terms in the balance (which are 200 to 400 cm/s/month). Note also that both the net vertical mixing tendency (wind-stress plus vertical mixing at 30 m) and the net nonlinear tendencies undergo

changes during the year that are much larger than the seasonal accelerations. Thus the seasonal cycle we seek to understand involves a small difference between several large terms, each of which varies significantly during a typical year.

The accelerations that produce the spring-time current reversal begin in early February (when $\partial u_s/\partial t$ first becomes positive). The acceleration remains positive (i.e. eastward) until mid-May. The current itself is most strongly positive during April–June. The pressure gradient tendency ($-\rho^{-1}\partial p_s/\partial x$) acts always to accelerate the zonal current to the east, while the net vertical mixing (D_{Zs}) always acts to accelerate the zonal current to the west. The pressure gradient tendency is relatively constant during the spring. D_{Zs} becomes smaller and reaches a minimum in late March, coincident with the wind-stress minimum. If these two terms balanced, the dynamics would describe a near-surface-layer equatorial Sverdrup balance. But there is an $O(1)$ imbalance between the two terms over this layer of fluid, with the acceleration tendency $\partial u_s/\partial t$ small compared with this imbalance. Let us now examine the other terms that comprise the remainder of the imbalance.

The nonlinear effect of the seasonal advection by the seasonal flow (NLA_s) is also to accelerate the flow eastward throughout the year. As well as being of opposite sign to D_{Zs} NLA_s tends to vary inversely with D_{Zs} over the first half of the year. NLA_s has the same order of magnitude as the eastward pressure gradient tendency. The nonlinear effect of the TIWs (NLA_{TIW}) is to accelerate the flow westward when TIWs are active; in the annual mean, this is the 'negative viscosity' effect of the TIWs near the surface that was discussed in HRH. There is strong seasonal variation in NLA_{TIW}; it varies from about 150 cm/s/month when the TIWs are strong to about 10 cm/s/month when the TIWs are weak. The westward tendency of NLA_{TIW} begins to weaken in early February, coincident with the springtime acceleration. As noted above, the reversal of u_s doesn't begin until late February. The strong TIW activity later in the year (Aug.–Sept.) is balanced primarily by a pronounced change in the net vertical mixing of momentum (D_{zs}); the Richardson-number dependent vertical mixing is enhanced by the near-surface current shears generated by the TIW activity. The acceleration term $\partial u_s/\partial t$ changes sign and the westward surface current weakens again briefly in November, when NLA_{TIW} is small.

During the boreal springtime period of eastward acceleration the contribution from NLA_{TIW} is necessary to make the acceleration large enough to reverse the near-surface current into eastward flow. The total acceleration resulting from the other momentum equation terms with eastward tendency, integrated over the period of positive $\partial u_s/\partial t$, is not enough to create eastward flow. In summary, the boreal spring eastward acceleration, which leads to the reversal of the surface current, needs both the weakening of the easterly zonal stress and the weakening of the instability waves (with the consequent reduction of their westward zonal momentum tendency) to produce the eastward surge.

It is of interest to decompose the pressure gradient and nonlinear tendencies to further elucidate the dynamics of the 0–30 m region. We see from Figure 6, which shows the components of NLA_s (seasonal advection of the seasonal flow, vertically averaged from the surface to 30 m depth), that the vertical advective term ($-w_s\partial u_s/\partial z$) is dominant, and

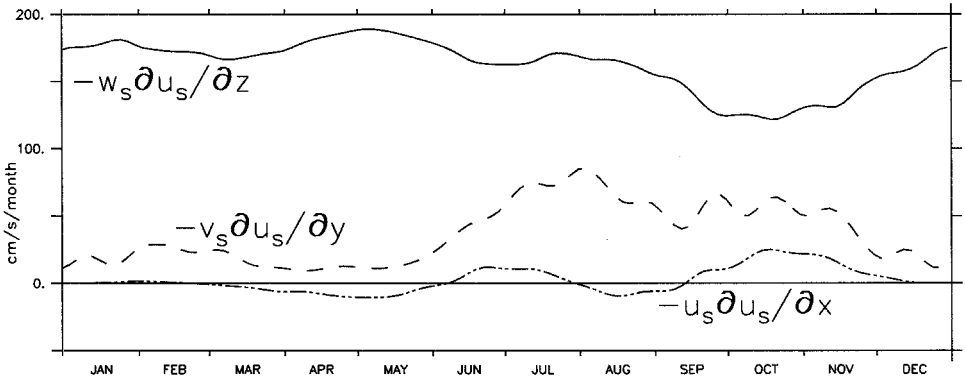

Figure 6. Nonlinear tendencies $-u_s\partial u_s/\partial x$, $-v_s\partial u_s/\partial y$ and $-w_s\partial u_s/\partial z$ in the seasonally-filtered zonal momentum equation, representing the seasonal advection by the seasonal flow (Eq. 7 in text). Terms are shown for one model year of the seasonal cycle, at one point (140W, 0N), averaged over $z = 0$–30 m depth. Units are cm/s/month, with the convention that positive values imply a tendency toward positive $\partial u_s/\partial t$.

contributes a surface eastward acceleration tendency throughout the winter and spring seasons. Wind-driven upwelling along the equator brings eastward-moving water from the EUC toward the surface, and thus acts oppositely to the surface easterly wind forcing. The meridional advective term ($-v_s\partial u_s/\partial y$) does not balance the vertical advective term, and the net nonlinear terms do not balance to $O(1)$. However, variations in NLA_s, as we saw above, do not contribute much to the springtime reversal. Figure 7 shows the three components of $\mathrm{NLA}_{\mathrm{TIW}}$, the TIW Reynolds stress contribution to the nonlinear driving,

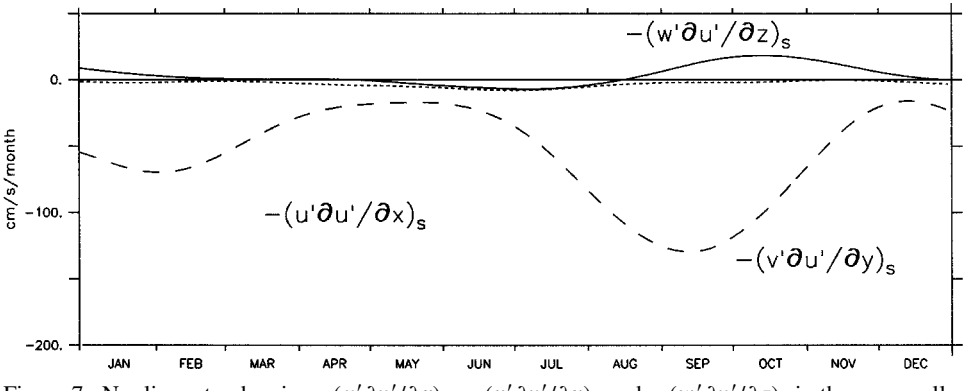

Figure 7. Nonlinear tendencies $-(u'\partial u'/\partial x)_s$, $-(v'\partial u'/\partial y)_s$ and $-(w'\partial u'/\partial z)_s$ in the seasonally-filtered zonal momentum equation, representing the TIW Reynolds stress contribution to the nonlinear driving (Eq. 8 in text). Terms are shown for one model year of the seasonal cycle, at one point (140W, 0N), averaged over $z = 0$–30 m depth. Units are cm/s/month, with the convention that positive values imply a tendency toward positive $\partial u_s/\partial t$.

vertically integrated from the surface to 30 m depth. The weakening of the meridional advection term $-(v'\partial u'/\partial y)_s$ associated with the TIW activity is seen to be the primary source of the spring TIW tendency for eastward acceleration.

Finally, Figure 8 shows the contributions at (140W, 0N) to the zonal momentum balance by surface $[-\rho^{-1}(\partial p_{\text{surface}}/\partial x)_s]$ and vertically averaged baroclinic $[-\rho^{-1}(\partial p_{\text{baroclinic}}/\partial x)_s]$ pressure gradient tendencies.[4] The surface pressure gradient tendency dominates; the baroclinic pressure gradient tendency changes are of the opposite sign and smaller. There are substantial changes in the surface pressure gradient over the course of the year. It is largest (~190 cm/s/month eastward) in November and weakest (~110 cm/s/month eastward) in July. The largest changes in the pressure gradient are its decrease from May to its July minimum, and the subsequent increase to its November peak. Through the spring period of eastward acceleration, it initially decreases from ~140 cm/s/month to 130 cm s^{-1} $month^{-1}$ in mid-March, it then returns to ~140 cm/s/month by mid-May.

Now consider briefly the balances that determine the post-May evolution of the near-surface flow. First let us examine the period from June through July that ends the eastward surge and returns the flow to its predominant westward direction. The wind-stress increases slightly and so does the total vertical mixing term (D_{Zs}); the pressure gradient is decreasing and the TIW contribution to the tendency is increasing. Each of these contributes westward acceleration; the TIW term has the largest change. The reduction of the zonal pressure gradient results principally from remote forcing from the west. Much of the westward acceleration tendency is counterbalanced by a significant increase of eastward acceleration tendency in the net seasonal nonlinear term. Almost all of the increase in seasonal nonlinearity results from changes in seasonal meridional advection.

Once the near-surface flow returns westward, it remains westward for the rest of the year; the net acceleration does not again become significantly positive (Fig. 5). This despite changes in the tendencies that are the largest in the seasonal cycle. For reasons we cannot rationalize, the strong tendency changes for eastward and westward acceleration never become significantly out of balance. Figure 6 shows that each of the advective components of the seasonal nonlinear tendency term undergo changes larger than $\partial u_s/\partial t$, with the largest changes in the meridional and vertical advection tendencies. Any observational program to examine the dynamics of the near-surface zonal flow must be capable of

4. Because the model does not explicitly compute the total zonal pressure gradient force, but only the baroclinic part, it is necessary to infer the barotropic (or "surface") part of the pressure gradient term. To accomplish this, we take the residual, over all the model-computed terms, from the zonal momentum balance at each time snapshot at 680 m (the 21st vertical level, well below the region of large time variation of zonal velocity) and take this to be the barotropic zonal pressure gradient force. This approach produces maximum imbalances in the annual mean equation of less than 3 cm/s/month (in the main thermocline), and typical imbalances of about 1 cm/s/month. If we had stored $\partial u/\partial t$ explicitly from the time-step calculation as it progressed, taking the barotropic pressure gradient as this residual could be done at any level and would be consistent with the internal numerics of the model; however we estimate $\partial u/\partial t$ from snapshots taken every 3 days and so inconsistencies arise whenever this is not an accurate approximation. Thus, it is important to take the residual from a grid location with the smallest $\partial u/\partial t$ values. The approach adopted by Wacongne (1990), in which a level of no motion is assumed to exist at 500 m, leads to imbalances typically of about 10 cm/s/month in the annual mean for this calculation.

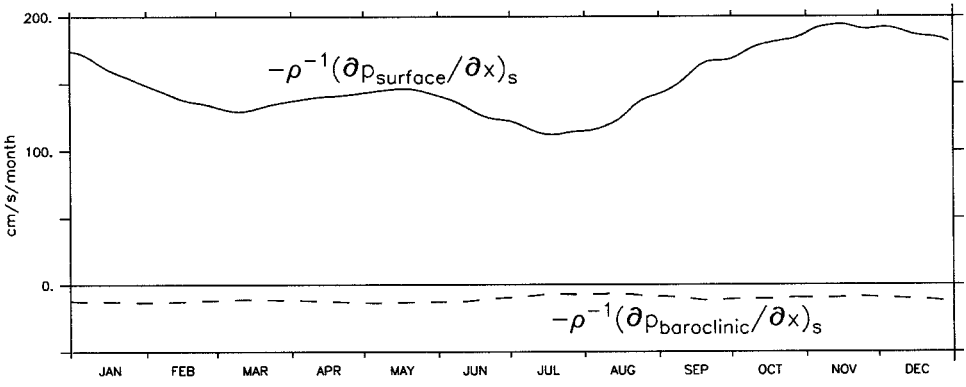

Figure 8. Zonal surface [barotropic; $-\rho^{-1}(\partial p_{surface}/\partial x)_s$] and baroclinic [$-\rho^{-1}(\partial p_{baroclinic}/\partial x)_s$] pressure gradient tendencies in the seasonally-filtered zonal momentum equation (see footnote 4 in text). Terms are shown for one model year of the seasonal cycle, at one point (140W, 0N). The barotropic term is obtained by taking the residual, over all the model-computed terms in the zonal momentum balance at each time snapshot at 680 m (the 21st vertical level, well below the region of large time variation of zonal velocity). The baroclinic term is averaged over z = 0–30 m depth. Units are cm/s/month, with the convention that positive values imply a tendency toward positive $\partial u_s/\partial t$.

making quite accurate estimates of all three of the advective terms (as well as of all the other terms in the zonal momentum equation), if the model flow behavior is representative of those in the ocean.

b. The depth-dependence of the momentum balances at (140W, 0N)

Figure 9 shows contour plots, at (140W, 0N) between the surface and 160 m depth, of the six main terms in the equatorial seasonally filtered zonal momentum equation: the local acceleration $\partial u_s/\partial t$, the pressure gradient tendency $-\rho^{-1}\partial p_s/\partial x$, the nonlinear advective terms NLA_s, and NLA_{TIW} (see Eqs. 6–8), and the mixing terms D_{Hs} and D_{Zs} (see Eqs. 4 and 5). Each of the terms undergoes seasonal variations of at least the same amplitude as $\partial u_s/\partial t$ (often they are much larger); the balances are fully nonlinear and include the model mixing processes. Every term in the equation appears in the basic balance of the seasonal cycle at some depth and time. Above the core of the EUC, the near-surface momentum balances described above basically hold. NLA_s and $-\rho^{-1}\partial p_s/\partial x$ tend to accelerate the flow eastward while D_{Hs} and D_{Zs} tend to accelerate the flow westward. The depth-dependence of NLA_{TIW} is consistent with the depth dependence of $\partial u_s/\partial t$, and the periods of positive acceleration of the zonal current correlate with the periods of TIW weakening. Below the core of the EUC, the TIW influence is weak, and NLA_s and $-\rho^{-1}\partial p_s/\partial x$ change sign through the seasons.

Figure 10 shows the terms that make up NLA_s and NLA_{TIW}. Near the surface (<20 m), $-v_s\partial u_s/\partial y$ (Fig. 10b) and $-w_s\partial u_s/\partial z$ (Fig. 10c) each contribute an eastward tendency.

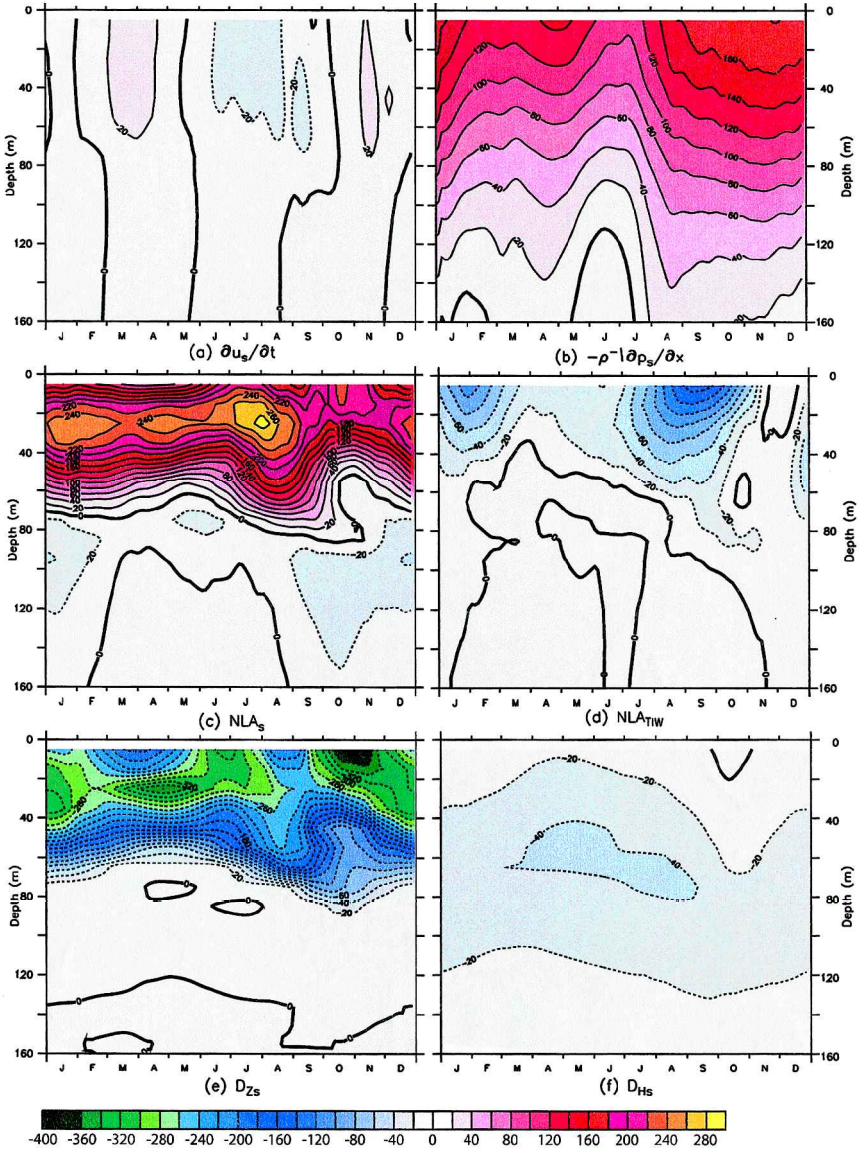

Figure 9. Contour plots at (140W, 0N) and between the surface and 160 m depth, of the six main terms in the equatorial seasonally filtered zonal momentum equation (Eq. 3 in text). (a) $\partial u_s/\partial t$; local acceleration, (b) $-\rho^{-1}\partial p_s/\partial x$; total pressure gradient, (c) NLA_s; seasonal advection by the seasonal flow (Eq. 7 in text) (d) NLA_{TIW}; TIW Reynolds stress contribution (Eq. 8 in text) (e) D_{Zs}; vertical mixing, which includes the wind-stress forcing (Eq. 5 in text), and (f) D_{Hs}; horizontal mixing (Eq. 4 in text). The tendencies are shown for one model year of the seasonal cycle, in units of cm/s/month, with the convention that positive values imply a tendency toward positive $\partial u_s/\partial t$. Contour intervals (see key) are the same for all panels.

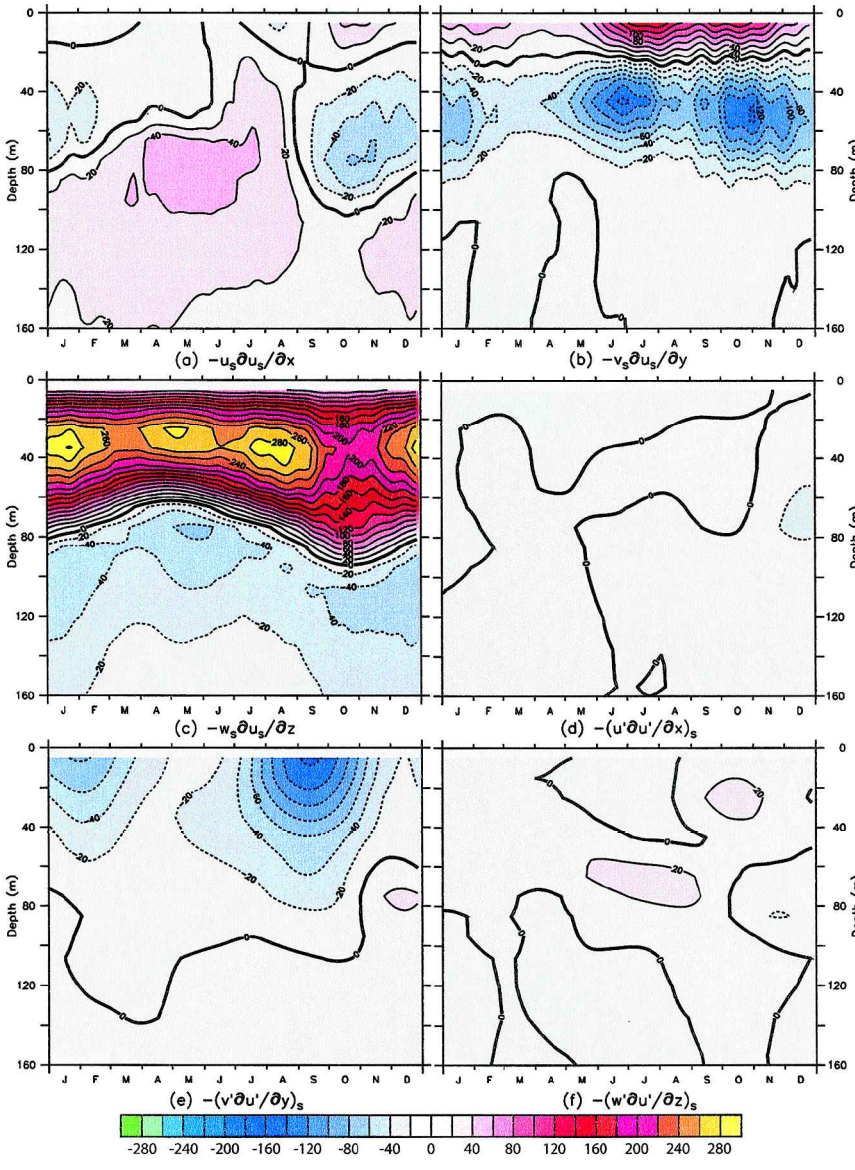

Figure 10. Contour plots at (140W, 0N) and between the surface and 160 m depth, of the individual nonlinear tendencies in the equatorial seasonally filtered zonal momentum equation (Eq. 3 in text): (a) $-u_s\partial u_s/\partial x$, (b) $-v_s\partial u_s/\partial y$ and (c) $-w_s\partial u_s/\partial z$, representing terms in the seasonal advection by the seasonal flow (Eq. 7 in text), and (d) $-(u'\partial u'/\partial x)_s$, (e) $-(v'\partial u'/\partial y)_s$ and (f) $-(w'\partial u'/\partial z)_s$, representing the TIW Reynolds stress contributions (Eq. 8 in text). The term balances are shown for one model year of the seasonal cycle, in units of cm/s/month, with the convention that positive values imply a tendency toward positive $\partial u_s/\partial t$. Contour intervals (see key) are the same for all panels.

Between 30 m and 80 m their tendencies oppose, with eastward vertical advection opposing westward meridional advection. Figures 10d–f show that there is no corresponding balancing tendency for the TIW component of the nonlinear term. The unbalanced $-(v'\partial u'/\partial y)_s$ instability wave tendency (Fig. 10e) has the same time-depth pattern as the spring time eastward acceleration (Fig. 9a). We here see the vertical structure of the TIW tendency terms in springtime.

In the Appendix we present the zonal momentum tendency terms as departures from the respective annual means; some readers may find it of interest to examine the changes that occur in each of the terms in Figures 9 and 10 in this format. For an observational process study of a particular period the results will likely be examined in the form of Figures 9 and 10. These figures indicate the levels at which it will likely be necessary to measure the momentum equation terms if we wish to explore observationally the mechanisms responsible for the seasonal cycle of zonal currents in the central equatorial Pacific. Every term must be known to at least 10 cm/s/month (and 5 cm/s/month would be preferable) if any useful balance is to be obtained.

c. The vertically integrated momentum balances at (140W, 0N)

Analyzing data from the Tropical Atmosphere Ocean Array (TOGA) during the 1980s and 1990s, YMb found that, for the seasonal cycle between 110W and 170W, the zonal surface wind-stress and baroclinic pressure gradient roughly provide a depth-integrated (0–250 m) zonal momentum balance (see Fig. 9 of YMb). In their analysis, differences between the stress and pressure gradient were roughly consistent with the local accelerations and decelerations of the zonal mass transport. Their maximum estimated nonlinear contribution to the balance is about 17% of the amplitude of the pressure gradient. QW found a similar result (see Fig. 19 of QW).

Figure 11a shows the model seasonal zonal momentum terms at (140W, 0N), vertically integrated over 0–250 m depth (reducing or extending the depth somewhat does not alter the results significantly). The nonlinear term has the same magnitude as the pressure gradient and vertical mixing terms. In the seasonal average, all the terms are important; the seasonal cycle is not in local equilibrium with the wind forcing. Figure 11b shows the residual of the wind-stress/vertical mixing minus the depth-integrated pressure gradient, and the depth-integrated local acceleration. This is our equivalent of the lower-right panels of Figure 9 from YMb. Their analysis shows an almost in-phase balance between these two quantities over the seasonal cycle; our results indicate a similar seasonal cycle, but the two effects do not balance.

There are several factors that may contribute to the difference between the zonal momentum balances inferred from the numerical model results and those estimated from data by YMb and QW. They are: (1) inability of the subsurface ADCPs to adequately observe the near-surface currents above 30 m (where the model says observations are critical), (2) coarse horizontal resolution of measurements (4 degrees in Longitude; 2 degrees in Latitude), which leads to inaccurate estimates for vertical velocity (QW), (3)

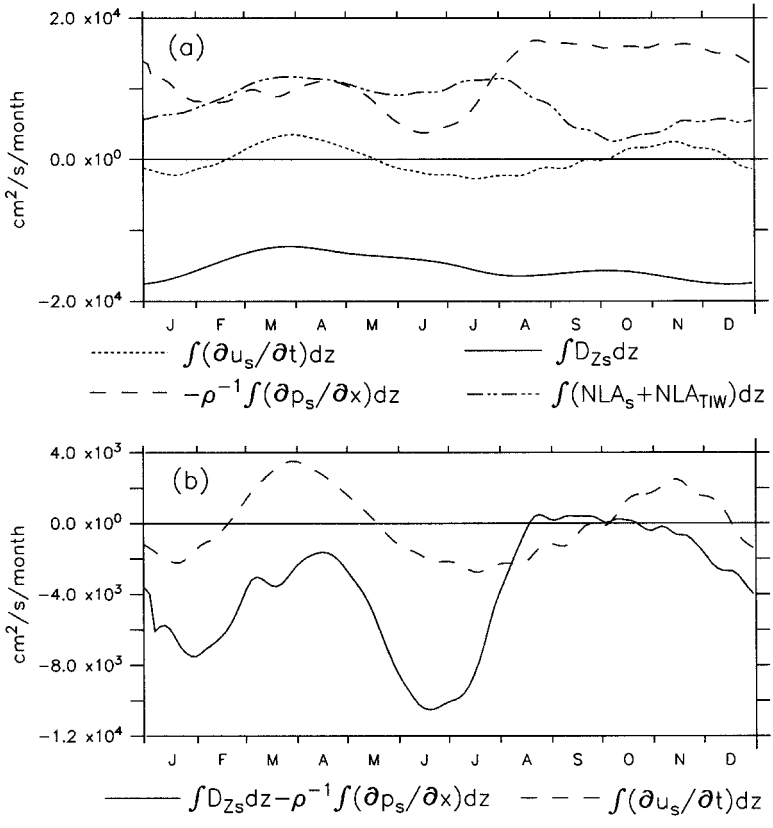

Figure 11. Model seasonal zonal momentum terms at (140W, 0N), vertically integrated over 0–250 m depth (reducing or extending the depth does not alter the results significantly). (a) The four major terms in the integrated momentum balance: integrated local acceleration $\int (\partial u_s/\partial t)dz$; integrated total pressure gradient $-\rho^{-1} \int (\partial p_s/\partial x)dz$; integrated total nonlinear terms $\int (\mathrm{NLA}_s + \mathrm{NLA}_{\mathrm{TIW}})dz$ (Eq. 6 in text); integrated vertical mixing (including wind-stress) $\int D_{Zs}dz$ (Eq. 5 in text). The term balances are shown for one model year of the seasonal cycle, in units of cm^2/s/month. (b) residual of the wind-stress/vertical mixing minus the depth-integrated pressure gradient, and the depth-integrated local acceleration. This is our equivalent of the lower-right panels of Figure 9 from Yu and McPhaden (1999b).

inability to compute $\partial/\partial y$ and w at all (we find that the terms not estimated in the YMb analysis are $O(1)$). To investigate the consequences of the vertical extrapolation done in each of the observational studies and of the horizontal differencing done in QW, we sampled our model u and v velocity fields as if they were ADCP data and then followed the data processing done in QW. Thus, u and v above 30 m were estimated by linear extrapolation based on the 30–40 m shear; then horizontal derivatives and the resulting estimate for w were computed on the relatively coarse TIWE mooring grid using the QW differencing and integration algorithm (described in the Appendix of QW). Figure 12a

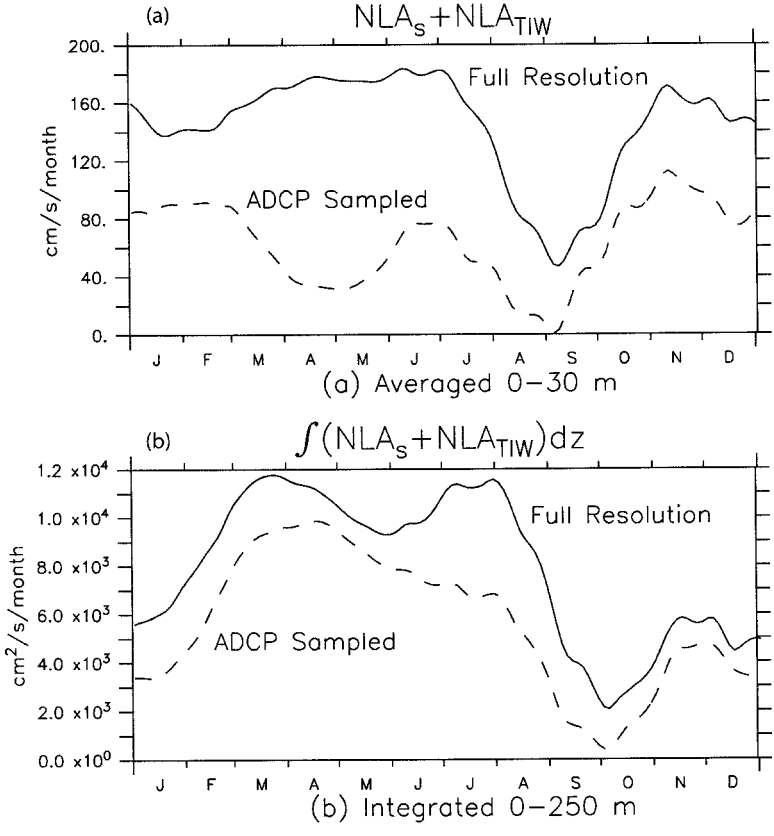

Figure 12. Comparison of 'ADCP-sampled' and 'full-resolution' model nonlinear terms at (140W, 0N). The ADCP-sampled velocities were obtained by using our model output u and v velocity fields, but u and v above 30 m were estimated by linear extrapolation using the 30–40 m shear. ADCP-sampled vertical velocity was computed by finite differencing the ADCP-sampled horizontal velocities on the coarse TIWE mooring grid. (a) The depth-averaged (0–30 m) ADCP-sampled nonlinear term is compared with its full-vertical resolution counterpart. (b) The vertically integrated (0–250 m depth) ADCP-sampled nonlinear term is compared with its full-vertical resolution counterpart.

compares these near-surface (0–30 m depth-averaged) 'ADCP-sampled' and 'full resolution' model nonlinear terms at (140W, 0N). The ADCP-sampled nonlinear contribution to the zonal momentum balance is reduced by more than a factor of two relative to the full model result. The vertically integrated ADCP-sampled nonlinear term is compared with its full-vertical resolution counterpart in Figure 12b; the ADCP-sampled nonlinear term contribution to the integrated momentum balance is greatly reduced during some time periods relative to the full model result.

This simple exploration does not establish that the model zonal momentum balances are correct or prove that the observational balances are incorrect. However, it raises the strong

possibility that experimental constraints associated with observations recently analyzed by QW and YMb in the equatorial Pacific Ocean may limit their ability to be definitive about near-surface current profiles and zonal momentum balances. It appears to be particularly inadvisable to attempt to make zonal momentum balance estimates simply from widely zonally spaced moorings, as was done by YMb.

4. The importance of instability waves

The zonal momentum balances described in this paper indicate that the seasonal changes in the model tropical instability waves (TIWs) play an important role in the creation of the eastward upper ocean flow in boreal spring. HRH showed that the TIWs act like a near-surface negative viscosity near the equator in the annual mean, in the sense that their zonal momentum tendency is to accelerate the westward near-surface mean flow westward. In our analysis here the loss of this westward tendency during boreal spring corresponds very closely to the eastward acceleration of the flow near the surface. There are other interesting correspondences between the TIW field's properties and the surface current eastward acceleration. A simple measure of the zonal and meridional structure of the model TIWs is the corresponding structure of the seasonally filtered $(u'v')_s$ momentum flux. Figures 13a–d show the longitudinal and latitudinal structure of the seasonally filtered zonal velocity u_s and the seasonally filtered TIW correlation $(u'v')_s$. There is an equatorial band (1S–2N) of TIW activity (Fig. 13d) extending from 110W to 180W, which is strongest between about 160W and 120W (Fig. 13c). Figures 13a and 13b show that the structure of the spring current reversal over a model year correlates very well with the longitudinal, latitudinal, and temporal structure of the weakening of the TIWs.

The best test we can construct to examine further the importance of the boreal spring TIW tendency changes (NLA_{TIW}) in the eastward surge is a series of additional numerical experiments with progressively weaker TIWs. A useful measure of the strength of the TIW tendency is the meridional structure of the annual mean of $u'v'$, since $\partial(u'v')_s/\partial y$ dominates the term. HRH's Figure 9 shows this field for our reference experiment, with its distinctive banded structure and peak values of $\sim 350\ cm^2\ s^{-2}$ just north of the Equator and $-275\ cm^2\ s^{-2}$ farther north. In our numerical ocean, raising the horizontal eddy viscosity reduces TIW energy (as noted by Philander *et al.,* 1986), but—for modest changes—does not strongly affect the mean EUC, SEC and NECC. Thus, we perform additional numerical experiments with A_m set at 2×10^7, 4×10^7, and $8 \times 10^7\ cm^2\ s^{-1}$ (recall that the initial model A_m was set to $1 \times 10^7\ cm^2\ s^{-1}$); we found that the maximum values of annual mean $u'v'$ decreased to about $150\ cm^2\ s^{-2}$, $50\ cm^2\ s^{-2}$ and $20\ cm^2\ s^{-2}$ for each successive experiment.

The eastward surge in the first experiment had only about half the peak eastward flow of the reference experiment. Neither of the other experiments, with still weaker TIWs, exhibits eastward flow. Because the imposed easterly winds weaken identically in every one of these experiments, D_{Zs} is similar in each of them; there also were no noteworthy changes in the pressure gradient. The seasonal nonlinear tendency term becomes smaller as

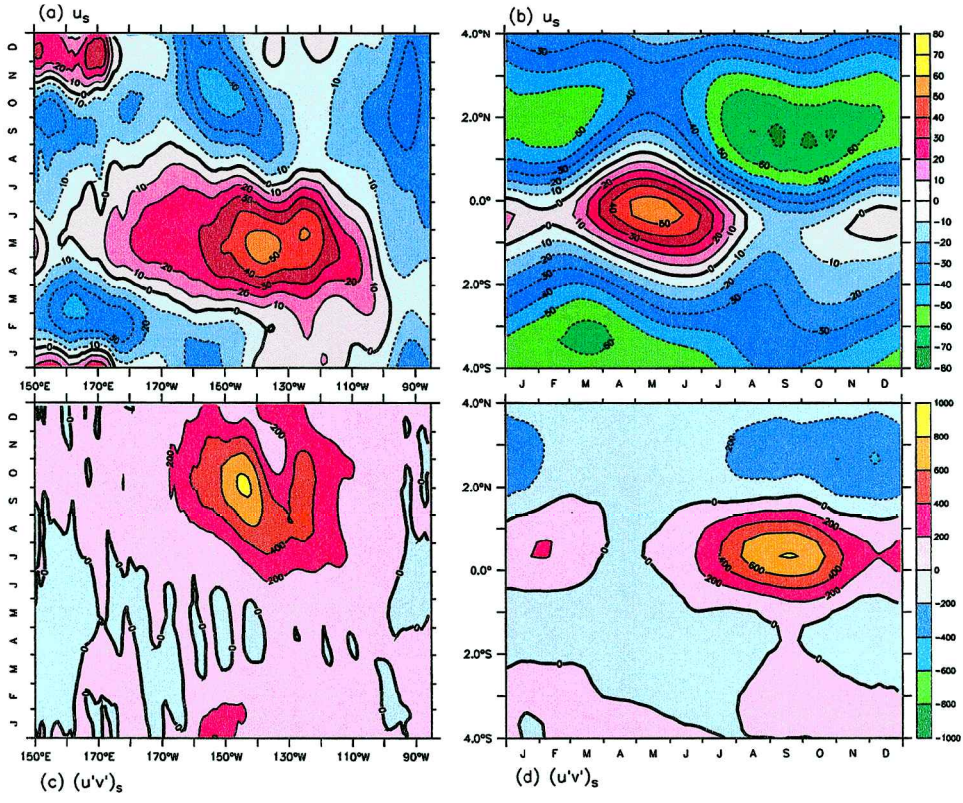

Figure 13. (a) Longitudinal structure (150E–85W) of seasonal cycle of seasonally filtered zonal velocity u_s (cm/s) at 0N, (b) Latitudinal structure (4S–4N) of u_s at 140W, (c) Longitudinal structure (150E–85W) of seasonal cycle of seasonally filtered TIW correlation $(u'v')_s$ (cm^2/s^2) at 0N, (d) Latitudinal structure (4S–4N) of $(u'v')_s$ at 140W. 'Cool' colors denote positive values (westward flow for u_s); 'warm' colors denote negative values (eastward flow for u_s). Key for (a) and (b) is shown in panel (b); key for (c) and (d) is shown in panel (d).

the friction is increased but its seasonal changes remain similar. As we saw in the reference experiment balances, there is not sufficient eastward near-surface acceleration from the springtime wind weakening alone to drive an eastward near-surface jet. In this model ocean, the additional eastward acceleration provided in the springtime by the changes in the realistic-amplitude TIWs is crucial for there to be an eastward surge.

5. Discussion

HRH described the model annual average flow and its zonal momentum equation balances at (140W, 0°), and compared them with the available observational estimates by Yu and McPhaden (1999, "YMb") and Qiao and Weisberg (1997, "QW"). We have here

presented the seasonal cycle of the model flow and its zonal momentum equation tendency terms. The model flow resembles the observations in many respects, but differs somewhat in others; the near-surface model flow cannot be evaluated with confidence, because only extrapolated near-surface currents are available near the surface. In all, the model provides as representative a simulation as is known to us. The largest seasonal current changes occur in the upper 40 meters; only there are the changes $O(1)$ relative to the annual mean.

The model momentum equation balances are not simple, in their time evolution or in their depth dependence. Between the surface and 250 m, every term is $O(1)$ somewhere and at some point in the seasonal cycle. A comprehensive survey and discussion of each regime, even at this one location, is beyond the scope of a paper of reasonable length. Thus, we have concentrated our attention on the most striking aspect of the seasonal cycle in this region of the world's ocean: the boreal spring near-surface reversal into an eastward current surge.

In the model, a period of boreal spring eastward acceleration leads to the reversal of the surface current. This period of acceleration results from the seasonal weakening of the easterly wind-stress and the seasonal weakening of the zonal momentum tendency from the Tropical Instability Waves (TIWs). The wind-stress alone is insufficient to create the eastward flow. We further explored the importance of TIWs in a series of experiments, each with diminishing TIW amplitudes. We found that the eastward surge first diminished and then failed to occur at all, as the TIW strength decreased. Clearly the association between the model instability waves and the eastward surge is strong. The springtime surface acceleration is not primarily the result of increased advection of eastward momentum from EUC water, decreased meridional seasonal circulation, or of remotely-forced changes in the zonal pressure gradient. Neither QW nor YMb discuss the dynamics of the springtime eastward surge, so these model results are offered as a hypothesis for future observational work to explore.

The main observational balance on which QW and YMb agree is that the vertically integrated between the surface and, say, 200 m is, to lowest order, between the wind-stress and zonal pressure gradient tendency terms. The model results differ decisively, having nonlinear effects as an $O(1)$ element of the balance. Over the near-surface depth range, which is not observed by the ADCPs used by QW and YMb, the model flow has strong horizontal divergence of mass, which leads to strong vertical velocity and vertical advection near the surface—just at the depth range where observations are not available. In Section 3, we presented an analysis that may explain the QW results. Using their observational constraints on the model output, nonlinear effects are greatly reduced and an approximate model Sverdrup balance exists. Until accurate measurements of the flow between the surface and about 30 m depth are available, from an array suitable for making accurate estimates of both the horizontal divergence and the advective terms, observational evaluation of this model result will remain impossible. However, the model results raise serious questions of whether we yet have knowledge of the basic depth-integrated and near-surface dynamics of the central equatorial Pacific zonal currents.

How do our results concerning the boreal spring eastward surge compare with other model results? Yu *et al.* (1997), using a different ocean model with less vertical resolution, were able to obtain a circulation that also exhibits eastward near-surface flow in the boreal spring. They do not provide zonal momentum equation diagnostics, but conclude "At this time (boreal spring) weakened local easterlies cause anomalous eastward flow that reverses the westward surface current and intensifies the EUC. Conversely, in late summer and fall strengthened local easterlies enhance the SEC and weaken the EUC (p. 323)." Our results indicate the local wind-stress changes are only part of the controlling balance. Philander and Chao (1991) suggest that upwelled eastward momentum, forced by winds west of 140W, is important to the eastward surge (p. 1405); we find little support for this suggestion in our analysis. In view of these differing interpretations, the need for new observational work to permit more careful evaluation of model currents and their balances is clear.

Tropical instability waves exist in the Pacific with amplitudes and estimated variances and covariances roughly similar to those found in the model experiment analyzed here (HRH). Analysis of dynamical aspects of the general circulation of the atmosphere has shown that amplifying disturbances in the atmosphere have a profound effect on the stability of zonal flow, transferring energy from zones of westerlies into zones of easterlies (e.g., Kuo, 1951). The unstable waves in the atmosphere are necessary elements both for developing and maintaining the zonal circulation and as braking mechanisms. If the ocean behaves as our experiment indicates, then the seasonal variations induced by the seasonal wind-stress variation play an equally important role in the unusual seasonal evolution of upper ocean equatorial currents in the central Pacific.

McPhaden and Taft (1988), discussing the observational dynamics of central and eastern equatorial currents, noted that the seasonal variation of the TIWs could produce seasonal tendencies consistent with a springtime increase—and subsequent decrease—in equatorial upper ocean eastward mass transport. They wrote, "These instabilities lead to an effective stress along the equator of $O(-10 \times 10^{-3}\ \mathrm{Nm}^{-2})$. (Hansen and Paul, 1984; Bryden *et al.,* 1986). Moreover, the amplitude of the instability is largest in boreal summer and fall and weakest in boreal spring." (See their p. 1731.) Such a stress is about 20% of the annual mean easterly stress at 140W. It may be useful to note that Hansen and Paul (1984), based on a quite limited data set, reported not only a different equatorial amplitude for the TIW Reynolds Stress from that reported by Bryden *et al.* (1986) but also an eastward mean near-surface current. The sign of the Hansen and Paul equatorial TIW tendency is of the opposite sign to that of Bryden *et al.* (1986). The Bryden *et al.* (1986) results are more consistent with more recent results (Johnson and Luther, 1990; Baturin and Niiler, 1997). HRH summarized the recent results. We have shown here that not only is the springtime change in TIW tendency consistent with the net acceleration observed from just above the core of the model EUC to the surface, it is essential to the springtime reversal of the near-surface flow from its normal westward direction.

Previous suggestions that the effect of the TIWs is dynamically similar to that of

horizontal mixing, and that numerical models with a resolution that is too coarse to resolve the eddies can simulate their effect by having a large coefficient for horizontal eddy viscosity (e.g., Philander *et al.,* 1986), are not consistent with the results reported here.

No effort has been made here to explore the detailed mechanisms of instability wave energy production or how they depend on the characteristics of the flow. In particular, we do not attempt here to investigate the flow changes that must occur in boreal winter that cause the seasonal weakening of the instability processes that drive the model TIWs. The meridional asymmetry associated with the TIWs seen in our model results is consistent with the conclusion of Yu *et al.* (1995), that TIW asymmetry is due mainly to the underlying asymmetry associated with the mean near-surface zonal currents. Cox (1980) carried out a careful study of such issues for a zonally averaged flow in one of the pioneering simulations of the tropical Pacific seasonal cycle. His results indicated the energy source was primarily barotropic instability, producing a most unstable channel mode with a zonal wavelength of about 1000 km and period of a little over 30 days. With our seasonal forcing, our TIWs behave similarly, except that the model TIWs here have a zonal wavelength of about 1500 km. However, Masina *et al.* (1999) analyzed TIWs in a numerical model of the Pacific Ocean similar to the one used here and found that the primary source of energy for the TIWs was a baroclinically unstable region north of the equator. The region of maximum instability was plausibly on the northern flank of the EUC and of the SEC just north of the EUC, at and above the depth of the EUC core. That result is consistent with the Luther and Johnson (1990) result (at 160W from the Hawaii-Tahiti Shuttle data set) that this is the primary energy source region. There is no indication here that the NECC or the vertical shear within the body of the EUC is involved importantly in the near equatorial instability wave effects examined here. Additionally, Cox (1980) found that the flow was unstable through the year, with weakest instability in boreal spring. The processes that control the timing, amplitude and Reynolds Stresses of the TIWs remain to be fully understood.

We speculate that the changes in the currents on the northern flank of the EUC and the adjacent part of the SEC that cause the system to become stable or only weakly unstable in boreal spring are wind forced, since the phase is correct and the changes in D_{Zs} down to about 60 m are in phase with the surface zonal wind-stress changes. Whether the primary control lies in the evolution of the equatorial SEC, the EUC (or both) deserves study. But a thorough study of realistic 3-D basic states of the equatorial Pacific remains to be done.

Could seasonal aspects of the model behavior associated with TIWs be evaluated with a intensive local dynamics process field experiment? The model budgets indicate that every term in the seasonal zonal momentum equation balance would have to be measured to a level of at least 10 cm s^{-1} $month^{-1}$ (5 cm s^{-1} $month^{-1}$ would be much better), including the vertical and horizontal mixing of zonal momentum. Such measurements would tax our capabilities, because they should be sustained for several years, but would be exceptionally interesting. A simpler and definitely feasible experiment would simply observe the horizontal current fields accurately on small enough spatial scales to define the shears,

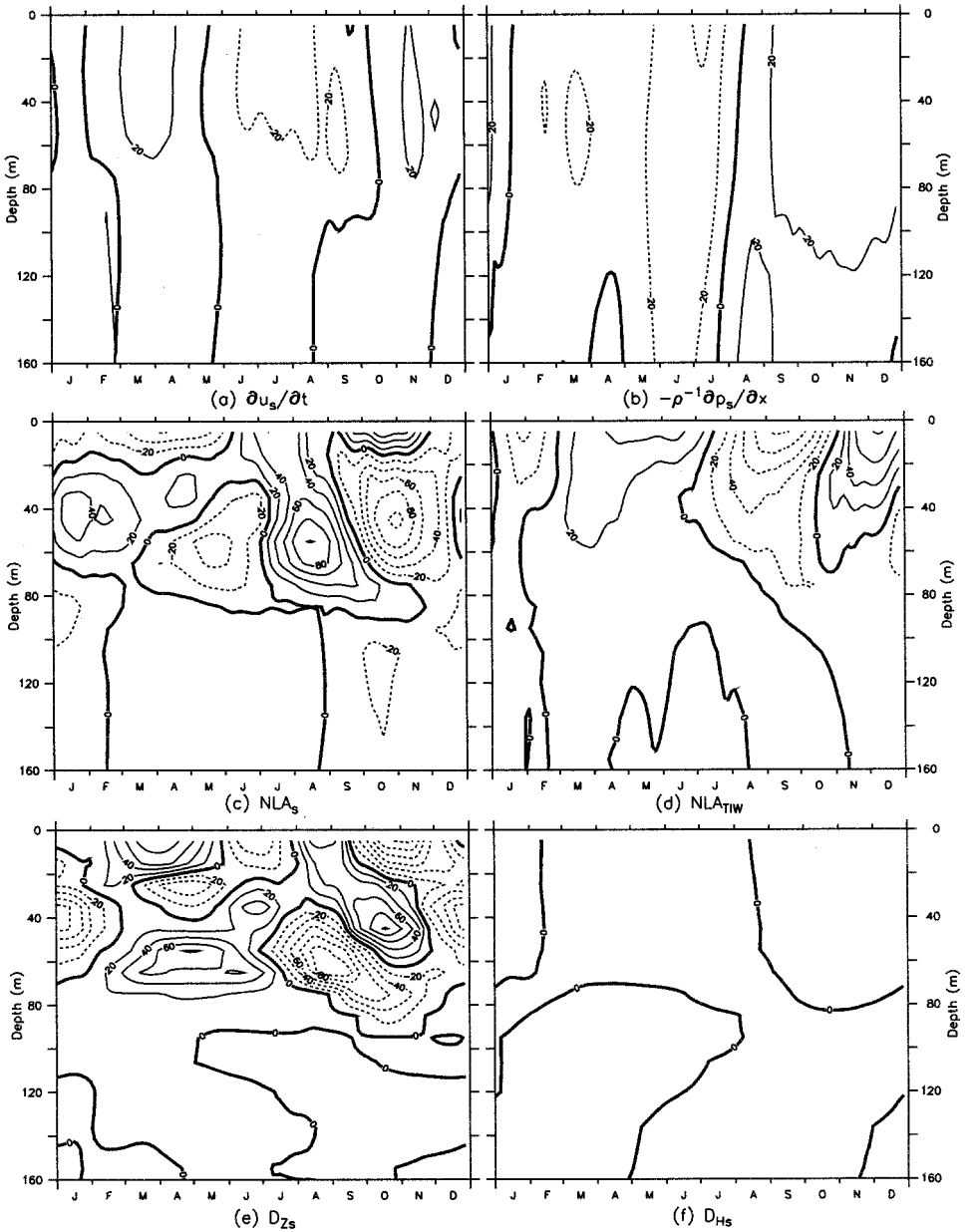

Figure 14. Contour plots at (140W, 0N) and between the surface and 160 m depth, of the six main terms in the equatorial seasonally filtered zonal momentum equation (Eq. 3 in text) minus their annual means. (a) $\partial u_s/\partial t$; local acceleration, (b) $-\rho^{-1}\partial p_s/\partial x$; total pressure gradient, (c) NLA_s; seasonal advection by the seasonal flow (Eq. 7 in text) (d) NLA_{TIW}; TIW Reynolds stress contribution (Eq. 8 in text) (e) D_{Zs}; vertical mixing, which includes the wind-stress forcing (Eq. 5 in text), and (f) D_{Hs}; horizontal mixing (Eq. 4 in text). The tendencies are shown for one model year of the seasonal cycle, in units of cm/s/month, with the convention that positive values imply a tendency toward positive $\partial u_s/\partial t$. Contour interval is 20 cm/s/month for all panels.

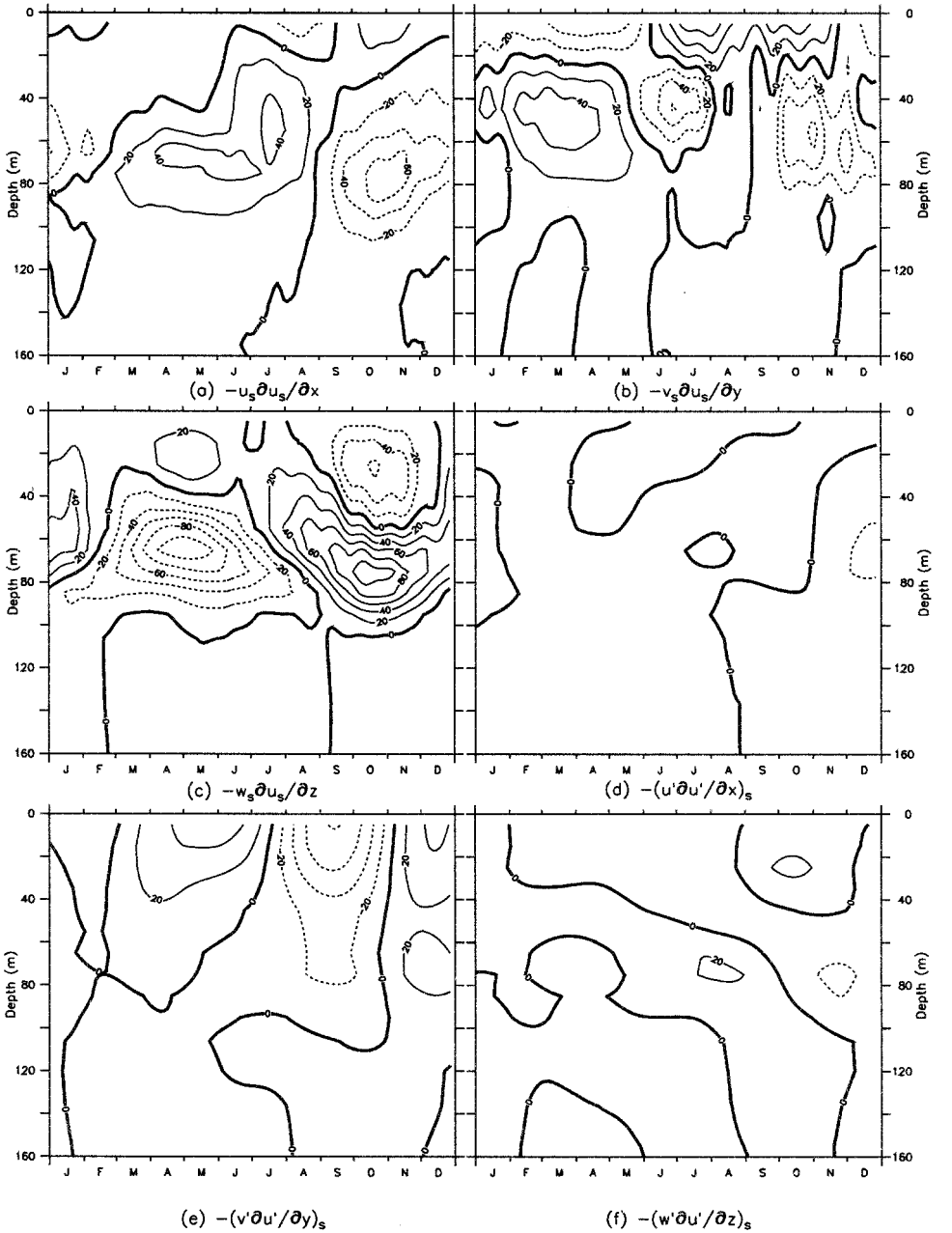

Figure 15. Contour plots at (140W, 0N) and between the surface and 160 m depth, of the individual nonlinear tendencies in the equatorial seasonally filtered zonal momentum equation (Eq. 3 in text) minus their annual means: (a) $-u_s\partial u_s/\partial x$, (b) $-v_s\partial u_s/\partial y$ and (c) $-w_s\partial u_s/\partial z$, representing terms in the seasonal advection by the seasonal flow (Eq. 7 in text), and (d) $-(u'\partial u'/\partial x)_s$, (e) $-(v'\partial u'/\partial y)_s$ and (f) $-(w'\partial u'/\partial z)_s$, representing the TIW Reynolds stress contributions (Eq. 8 in text). The term balances are shown for one model year of the seasonal cycle, in units of cm/s/month, with the convention that positive values imply a tendency toward positive $\partial u_s/\partial t$. Contour interval is 20 cm/s/month for all panels.

variances, covariances and curvature between about 2S and 5N (the region of maximum EUC/SEC/NECC structure). This flow information would provide crucial model flow validation information, and would provide data sufficient to avoid the shortcomings of previous field experiments. Until such time as this information is obtained, our community will be unable to evaluate the plausibility of different observational and numerical model results.

Acknowledgments. Special thanks to George Philander and Ron Pacanowski for developing and sharing their version of the Bryan-Semtner-Cox model and to Ron for helping us continue to use that basic set of physics through his Modular Ocean Model (MOM). DEH thanks Ed Sarachik for presenting these results at the Equatorial Theory Panel meeting at URI in 1991 and Zuojun Yu and Xuri Yu for many subsequent and usefully skeptical conversations. The Thermal Modeling and Analysis Project (TMAP) at PMEL provided programming assistance and the Ferret analysis program was used in the analysis of the model outputs (http://tmap.pmel.noaa.gov/ferret). Financial support for TMAP is provided by NOAA/PMEL, NOAA/OAR and NOAA/OGP and by NASA order # W-19,533 (Physical Oceanography). This is PMEL contribution # 2191 and JISAO publication #803.

APPENDIX

The zonal momentum equation terms, as departures from their annual means

As we note in the text, the seasonal variation of the zonal momentum tendency terms typically is small compared with the dominant balances that exist in the annual mean; to lowest order the annual mean balances hold throughout the year at most depths. Because we wish to facilitate comparison of the model tendency terms with the published observational tendency terms, in the text we have presented the terms in the forms in which they appear in the zonal momentum equation.

A different perspective on the seasonal cycle is obtained if the tendency terms, minus their annual mean values, are examined. Here we present the model zonal momentum equation terms in this fashion, for those who are interested in this alternative perspective (Figs. 14 and 15). It is important, in looking at the figures presented here, to remember not to associate positive and negative values with eastward and westward zonal momentum tendencies; the annual mean value must be added in order to determine the sign of the tendency. But these figures do make it easier to visualize the changes in each of the tendency terms that occur throughout the seasonal cycle of the model.

REFERENCES

Baturin, N. G. and P. P. Niiler. 1997. Effects of instability waves in the mixed layer of the equatorial Pacific. J. Geophys. Res., *102* (C13), 27,771–27,793.

Bryden, H. L., E. C. Brady and D. Halpern. 1986. Lateral mixing in the equatorial Pacific Ocean, *in* Further Progress in Equatorial Oceanography, E. Katz and J. Witte, eds., Nova University Press, 121–132.

Cox, M. D. 1980. Generation and propagation of 30-day waves in a numerical model of the Pacific. J. Phys. Oceanogr., *10,* 1168–1186.

Gill, A. E. 1982. Atmosphere-Ocean Dynamics, Academic Press, 662 pp.

Hansen, D. V. and C. A. Paul. 1984. Genesis and effects of long waves in the equatorial Pacific. J. Geophys. Res., *89* (C6), 10431–10440.

Harrison, D. E., R. D. Romea and S. H. Hankin. 2001. Central equatorial Pacific zonal currents. I: The Sverdrup balance, nonlinearity and tropical instability waves. Annual mean dynamics. J. Mar. Res., *59,* 895–919, (this issue).

Johnson, Eric S. and Douglas S. Luther. 1994. Mean zonal momentum balance in the upper and central equatorial Pacific Ocean. J. Geophys. Res., (C4) *99,* 7689–7705.

Kuo, H. L. 1951. Dynamical aspects of the general circulation and the stability of zonal flow. Tellus, *3,* 268–284.

Luther, D. S. and E. S. Johnson. 1990. Eddy energetics in the upper equatorial Pacific during the Hawaii-to-Tahiti shuttle experiment. J. Phys. Oceanogr., *20,* 913–944.

Masina, S., S. G. H. Philander, and A. B. G. Bush. 1999. An analysis of tropical instability waves in a numerical model of the Pacific Ocean 2. Generation and energetics of the waves. J. Geophys. Res., *104* (C12), 29637–29661.

McPhaden, M. J. 1993. TOGA-TAO and the 1991–93 El Nino Southern Oscillation Event. Oceanography, *6,* 36–44.

McPhaden, M. J. and S. P. Hayes. 1990. Variability in the eastern equatorial Pacific during 1986–88. J. Geophys. Res., *95,* 13,195–13,208.

McPhaden, Michael J. and Bruce J. Taft. 1988. Dynamics of seasonal and intraseasonal variability in the eastern equatorial Pacific. J. Phys. Oceanogr., *18,* 1713–1732.

Pacanowski, R. C. 1995. MOM 2 Documentation, User's Guide and Reference Manual, Version 1.0, Sept 30, 1995, GFDL Ocean Technical Report #3.

Philander, S. G. H. and Y. Chao. 1991. On the contrast between the seasonal cycles of the equatorial Atlantic and Pacific oceans. J. Phys. Oceanogr., *21,* 1399–1406.

Philander, S. G. H., W. J. Hurlin and R. C. Pacanowski. 1986. Properties of long equatorial waves in models of the seasonal cycle in the tropical Atlantic and Pacific oceans. J. Geophys. Res., *91,* 14,207–14,211.

Philander, S. G. H., W. J. Hurlin and A. D. Siegel. 1987. Simulation of the seasonal cycle of the tropical Pacific Ocean. J. Phys. Oceanogr., *17,* 1986–2002.

Qiao, L. and R. H. Weisberg. 1997. The zonal momentum balance of the equatorial undercurrent in the central Pacific. J. Phys. Oceanogr., *27,* 1094–1119.

Sverdrup, H. U. 1947. Wind-driven currents in a baroclinic ocean, with applications to the equatorial currents of the eastern Pacific. Proc. Natl. Acad. Sci., U.S.A., *33,* 318–326.

Wacongne, S. 1990. On the difference in strength between Atlantic and Pacific undercurrents. J. Phys. Oceanogr., *20,* 792–799.

Wyrkti, K. and G. Meyers. 1976. The trade wind field over the Pacific Ocean. J. Applied Meteor., *15,* 698–704.

Yu, X and M. J. McPhaden. 1999a. Seasonal variability in the equatorial Pacific. J. Phys. Oceanogr., *29,* 925–947.

——— 1999b. Dynamical analysis of seasonal and interannual variability in the equatorial Pacific. J. Phys. Oceanogr., *29,* 2350–2369.

Yu, Z, J. P. McCreary Jr. and J. A. Proehl. 1995. Meridional asymmetry and energetics of tropical instability waves. J. Phys. Oceanogr., *25,* 2997–3007.

Yu, Z., P. S. Schopf and J. P. McCreary Jr. 1997. On the annual cycle of upper-ocean circulation in the eastern equatorial Pacific. J. Phys. Oceanogr., *27,* 309–324.

Received: *27 January, 2000;* revised: *11 September, 2001.*